Multi-physics modeling of industrial inductors associated to converters

G. Parent, M. Rossi, M. Hecquet, V. Lanfranchi* and M. Bekemans**
Université Lille Nord de France – Ecole Centrale de Lille – L2EP
*LEC, Université de technologie de Compiègne
**Alstom Transport Charleroi

Abstract — Acoustics comfort is an increasingly important factor at the design stage of industrial inductors associated to converters. In addition, power converters in railway domain are more and more compact and powerful. That is why the lumped models for the electromagnetic, thermic and vibro-acoustic parts are developed.

This aim of this paper is to detail the multi-physical model in order to design the industrial inductors for traction applications.

I. INTRODUCTION

The design process of such components becomes more and more multi-physical. Effectively, the "miniaturization" leads to new design constraints, such as taking into account of the thermal issues due to many additional current harmonic in the windings [1], as well as the emission of sound.

Numerical tools, such as the well-known Finite Element Analysis (FEA), can be tremendously helpful in the design process, as far as they allow computing very accurate models in a vast range of physical domains. Nevertheless, the more accurate is the required solution, the more time-consuming is the computation, especially in the case of coupled problems. This last point is particularly penalizing in an optimization process.

Hence, lumped models are detailed and used in order to get a good compromise between accuracy and time computing. In this paper, three lumped models are proposed. A nodal network and a spring-mass model are developed for the thermal and the vibro-acoustic parts respectively.

II. MULTI-PHYSICS MODELING

Magnetic components, such as transformers and industrial inductors, bring into play a vast range of physical domains, such as electromagnetic, thermic and, in a lesser way, acoustic. All those physical phenomena interact onto each other, in a more or less strong way. A meaningful example is the winding temperature that changes its resistance and so Joule losses, and so on. Hence, any design process has to be taken into consideration by a multi-physical point of view. As an illustration, a synthesis of the different physical domains and their interactions between each other is shown in Fig. 1.

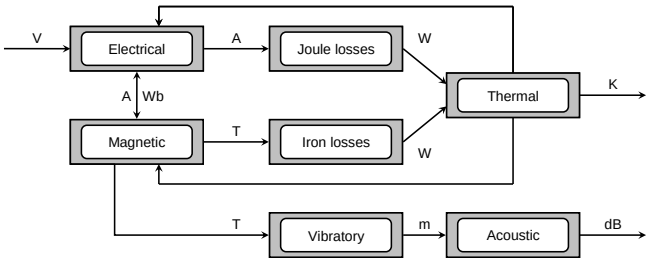

Fig. 1: Multi-physics domains and their interactions

A. Electromagnetism

That it is a thermal or a vibro-acoustic computation, the source quantity is provided by an electromagnetic computation. In a design process, the induction value as well as the current harmonics values are design specifications, and thus set by designers. Hence, in our study, the electromagnetic model is simplified: the induction is set to the saturation limit and the current harmonics are assumed known.

As shown in Fig. 1, the sources of the thermal problem are iron losses and Joule losses.

The iron losses (P_c) computation is based on the Steinmetz model. Formula (1) is an empirical equation allowing taking into consideration both the hysteresis and the eddy current phenomena.

$$P_c = K_c f^{\alpha} B^{\beta} V_c \tag{1}$$

Where f is the frequency, B the induction and V_c the volume of the iron core. α, β and K_c are coefficient easily to estimate by performing a linear regression on losses curves given in steel manufacturer's datasheets. To properly take into account harmonics, P_c is calculated for each one and the total iron losses are evaluated by summing all the so calculated P_c.

Joule's law allows computing Joule losses P_w (3), which only depends on the current I_{eff}, the winding electrical resistance R_{DC} and the F_r ratio to take into account of the proximity and skin effects [2],[3].

$$F_r = \frac{R_{ac}}{R_{dc}} \tag{2}$$

$$P_w = F_r \cdot R_{dc} \cdot I_{eff}^{\ 2} \tag{3}$$

978-1-4244-8218-4/10/$26.00 ©2010 IEEE

The winding resistance at low frequency R_{dc} is not very well known by manufacturers and the more often it had to be re-adjusted by experimental measurements. A detailed method of determination of R_{DC} using Bezier curves is given [7].

Losses calculation of the inductor has been compared to experimental measurement. Using an impedance analyzer, the real part of the inductor impedance has been measured. The electrical model is presented in the Fig. 2 and results are shown in Fig. 3. R_w, R_m, X_f and X_m are respectively the winding resistance, the iron losses, the leakage inductance and the magnetizing inductance.

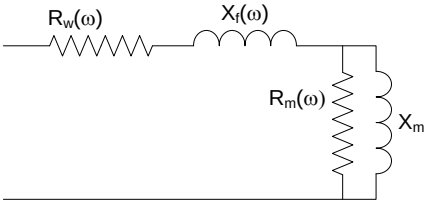

Fig. 2: electromagnetic equivalent model

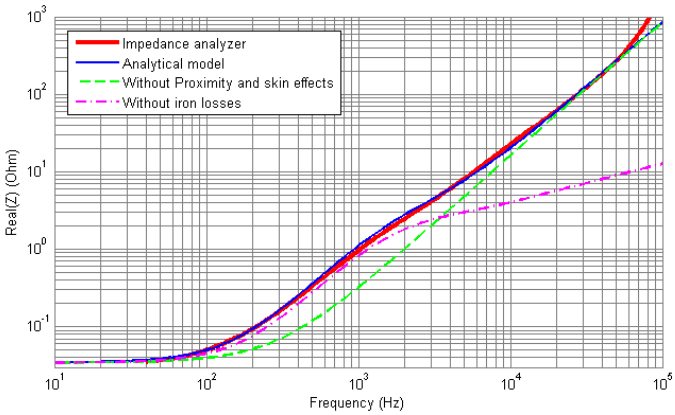

Fig. 3: Comparison between the real part of the inductor impedance and the electromagnetic model

To obtain accurate precision at high frequency, it is necessary to well-known Steinmetz parameters because R_μ is function of: $f^{(\beta-\alpha)}$, so the difference between this two parameters gives the final slope of the curve.

In the case of a vibro-acoustic model, the source term is the magnetic force (Fig. 1).

In a magnetic core, two different kinds of forces can appear from a magnetization: magnetostriction forces inside the core and Maxwell forces at the iron/air interface [9]. Contrary to transformers, industrial inductors, like electrical machines, have air gaps. Hence, in those systems, magnetostriction forces are neglectable compared to Maxwell forces. The force density can be expressed as follows:

$$F(t) = \frac{[B(t)]^2}{2\mu_0} \quad (4)$$

III. Thermal Model

Thermal study in a transformer can be separated in three phenomena: conduction, forced convection and radiation. The latter can be neglected in the case of air-forced cooling [4]. Moreover, on our study, only the steady-state is considered, allowing the suppression of thermal capacitances from the model.

The aims of this thermal model are the ability to evaluate the temperature in three parts of the system: in each layer of the winding along the core, inside the core and in the air ducts according to their size and position. Since analytical models can only supply average temperature [5],[6], a 3D nodal network approach has been chosen for the thermal simulation.

In term of industrial inductors, vast range geometry exists. Hence, the flexibility of the network construction is important so it has the ability to adapt the network to the system geometry. An algorithm has been implemented to generate automatically the network of one of the industrial inductor's column with its windings and air ducts. Moreover, the network should be adapted to give the temperature of each column in two plans as shown in Fig. 4.

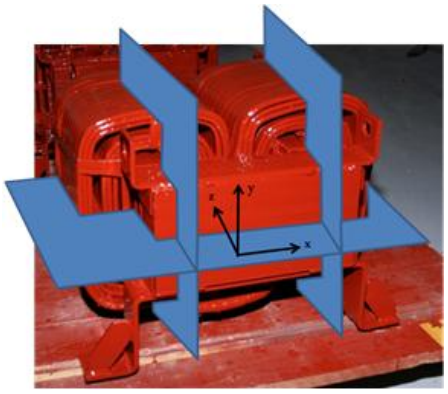

Fig. 4: plans of thermal study in the case of a DC inductor

Each turn of winding is divided in four thermal resistances which are connected together as a coil as seen in Fig. 5. This topology describes the possibility of heat flux to move along the copper. To class the elements, a cylindrical coordinate system (m,n,p) is placed (Fig. 5), where *n* is an axial vector to the core while *m* and *p* are the argument and length of a node in the radial plan respectively.

These parameters are discrete values. *m* and *n* are natural integers and represent the layer and turn numbers respectively. As a turn is divided in four elements, *p* is defined so that $p \in \left\{0; \frac{\pi}{2}; \pi; \frac{3\pi}{2}\right\}$ .For example, the resistances R_w is saved in a matrix $R_w(m,n,p)$. As same for resistances, the temperatures of winding T_w use the same classification as R_w.

The heat flux in the coil also has the possibility to cross the conductor insulation to join directly the next turn, which is why resistances R_n are placed in the network. Each node

is connected to a heat flux source P_j to insert Joule losses. (Sources are not represented in Fig. 5 and Fig. 6).

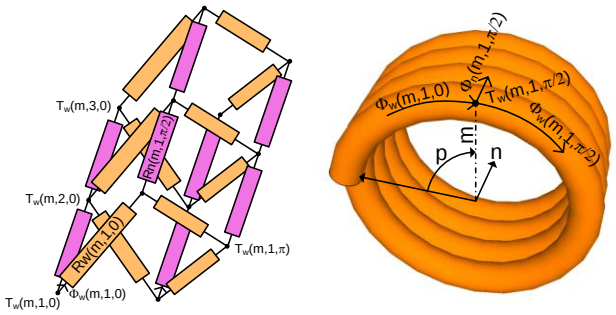

Fig. 5: part of the 3D Network of a layer of winding

In order to simplify the mathematical equations, the following assumption (5) is used, so equations (6) are extracted from the electrical network.

$$\begin{cases} \Delta_m T_i(m,n,p) = T_i(m+1,n,p) - T_i(m,n,p) \\ \Delta_n T_i(m,n,p) = T_i(m,n+1,p) - T_i(m,n,p) \\ \Delta_p T_i(m,n,p) = T_i(m,n,p+\pi/2) - T_i(m,n,p) \end{cases} \quad (5)$$

$$\begin{cases} \Delta_n T_w(m,n,p) = R_n(m,n,p) \times \Phi_n(m,n,p) \\ \Delta_p T_w(m,n,p) = R_w(m,n,p) \times \Phi_w(m,n,p) \end{cases} \quad (6)$$

Since layers are not isotherms, the heat flux is able to cross to a next layer or to an air duct. In order to take this phenomenon into account, each node has the possibility to receive or transfer heat flux by adjoining Φ_{mi} (input) and Φ_{mo} (output) thermal flux and resistances R_m (Fig. 6).

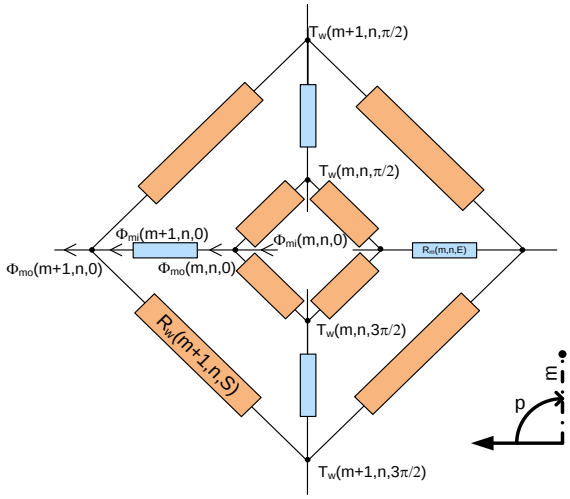

Fig. 6: network between two layers

For two following layers, equations (7) are applied. In this case, a variable of current is redundant and an equality of variable is done.

$$\begin{cases} \Delta_m T_w = -R_m(m,n,p) \times \Phi_{mo}(m,n,p) \\ \Phi_{mo}(m,n,p) = \Phi_{mi}(m+1,n,p) \end{cases} \quad (7)$$

If two consecutive layers are separated by an air duct, equations (8) are applied

$$\begin{cases} \Delta_n T_{air} = R_{air}(m,n,p) \times \left[\Phi_{mo}(m,n,p) - \Phi_{mi}(m+1,n,p)\right] \\ T_{air}(d,n,p) - T_{air}(m,n,p) = -R_m(m,n,p) \times \Phi_{mo}(m,n,p) \\ T_{air}(d,n,p) - T_{air}(m+1,n,p) = -R_m(m+1,n,p) \times \Phi_{mi}(m+1,n,p) \end{cases} \quad (8)$$

The temperature in air ducts is stored in the matrix $T_{air}(d,n,p)$ where *d* is the number of the duct. In this case, resistances R_m are a mix of conduction and convection.

For the magnetic core, the network shown in Fig. 7 is used.

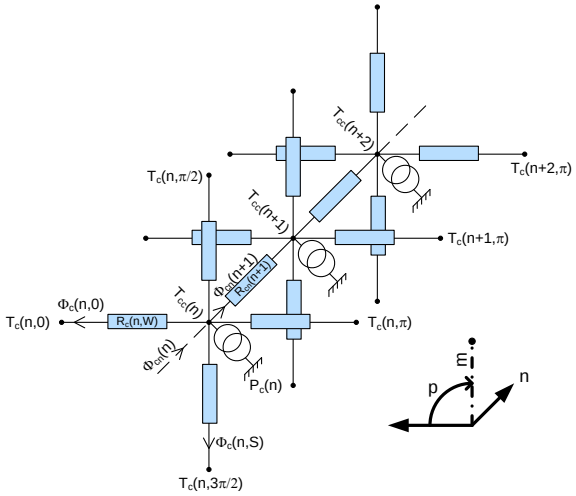

Fig. 7: network for the magnetic core

The network can take into account different conductivity coefficient, depending on the direction. This is important due to the nature of the core which is built from thin metal sheets stacked but insulated from each others. Hence, the conductivity decreases in the stacking direction. In Fig. 7, $T_{cc}(n)$ is the temperature middle of the core, $T_c(n,p)$ is the temperature at the edge of the core and $P_c(n)$ represents the iron losses.

This network gives the following equations:

$$\begin{cases} T_{cc}(n+1) - T_{cc}(n) = R_{cn}(n) \times \Phi_{cn}(n) \\ T_{cc}(n) - T_c(n,p) = \times R_c(n,p) \times \Phi_c(n,p) \end{cases} \quad (9)$$

The core network can directly be connected to a layer by using (6) or to an air duct by using (7), and by swapping $\Phi_{mo}(m,n,p)$ and $\Phi_w(m,n,p)$ by $\Phi_c(n,p)$ and $\Phi_c(n,p)$ respectively.

For each node of the network, the Kirchhoff's current law is applied as shown by (10), where Φ_i are the current in the branches of the node and P_i is the source of losses.

$$\sum_i \Phi_i + P_i = 0 \tag{10}$$

The thermal model has been tested on the inductor and results are exposed on the Fig. 8 and error is less than 5% compare to experimental measurement using thermocouple positioned in the winding. The representation is based on the plans introduced in Fig. 4.

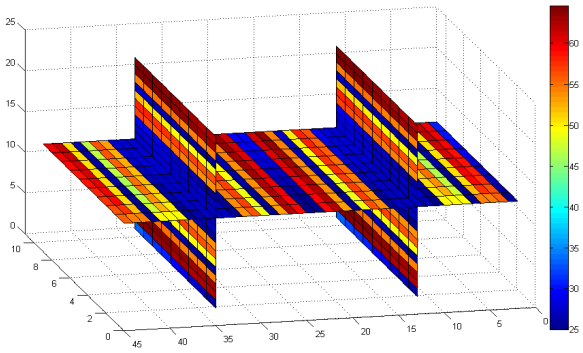

Fig. 8: Gradient temperature estimated with the thermal model

IV. VIBRO-ACOUSTIC MODEL

Every electromagnetic system is subject to vibrations, and thus to emission of sound. It is well known that in electrical machines, deflections in the exciting mode are due to the Maxwell forces that are applied on the inner surface of the stator [8]. In transformers, the noise source can be split into two different cases: the "Core noise", caused by magnetostriction in the core steel laminations, and the "Load noise" caused by electromagnetic forces in the windings and structural parts [9], [10], [11].

Like in transformers, both magnetostriction forces in the core and electromagnetic forces in the windings are present in industrial inductors. In addition to those phenomena, Maxwell forces at the core/air interface are also present in the air gaps [12]. All those phenomena contribute to the emission of sound, but due to the ratio between magnetostriction, electromagnetic forces in the windings and Maxwell forces, this paper will deal only with the latter.

A. *Industrial Inductor Modal Analysis*

Any vibro-acoustic study starts with a conventional modal analysis. Indeed, such an analysis gives all possible resonance modes and their associated deflection shapes and frequencies. In the case of electromagnetic systems, this step is critical since alternative quantities, such as current and flux density for example, are involved and according to their frequencies, may incite the structure.

The conventional modal analysis can be performed through Finite Element (FE) simulations or measurements, using accelerometers and a roving hammer. Both methods have pros and cons. Indeed, FE simulations allow performing a lot of different cases in a small lapse of time just by changing some parameters. Nevertheless, two main difficulties appear in FE simulations. The first one is about the geometry of the model. In the case of industrial inductors, the real system is composed of a core, windings and some fixation parts, which can lead to complex FE models. The more often, only the core is taken into account in the FE model, which means that the resonance modes won't perfectly match the real system ones. The other difficulty is about setting the material properties and the prestress conditions to their proper values. In particular, the latter is pretty hard to determine since it is very variable from a system to another. For those reasons, the FE simulation is used to determine the influence of several parameters, such as the geometry, on the resonance modal deflections shapes.

On the other hand, measurements with accelerometers and a roving hammer give results associated to the *real* industrial inductor, including the core, the windings and the fixation parts. Nevertheless, the main problem encountered with this method is that a lot of places of the system are not reachable with the accelerometers.

For all these reasons, in our study, both methods have been used.

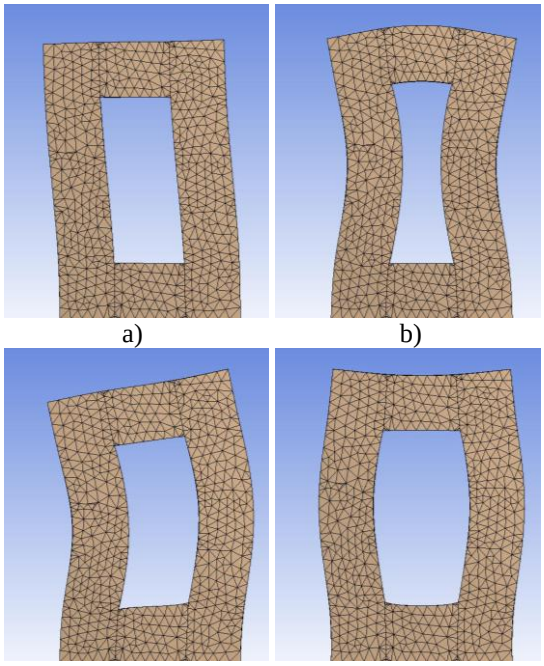

Fig. 9 : Four of the calculated in-plane resonance modes (maximum deflections)

Fig. 9 shows the four first in-plane resonance modes deflections calculated from a FE simulation.

Measurements with accelerometers and roving hammer give the same resonance modes deflections, among which one can notice an elliptical mode Fig. 9.b and a breathing mode Fig. 9.d. Nevertheless, for all the reasons we mentioned, the associated frequencies values are different.

B. *Industrial Inductor Operational Deflections Shapes*

A modal analysis gives all the possible resonance modes of a system. Nevertheless, the fact that a resonance mode is present doesn't mean that it will be incited in a normal use

of that system. Hence, in addition to a modal analysis, an Operational Deflection Shape (ODS) analysis has to be performed. The aim of the ODS allows:

- to know how the system *really* vibrate at a given frequency.
- to know which resonance mode is actually excited and which is not. This information is critical when the industrial inductor is associated to a power electronic converter, to choose a switching frequency for example.
- to link deflections shapes and noise emission levels, with an acoustic power measurement.

In our case, the ODS measurements have been performed on several "U/I" DC industrial inductors using Brüel & Kjaer ODS tools. The inductors were supplied by a classic chopper allowing choosing the switching frequency, and the measurements were performed as follows:

- first, the chopper switching frequency is swept from 0 Hz to 6kHz, and the acoustic power level is recorded. This measurement allows highlighting the sound emission levels pikes with respect to the switching frequency. Hence, the so obtained frequencies can e compared to the resonance modes ones.
- several ODS measurements are performed at fixed switching frequency. The latter are chosen according to the modal analysis and the measurements mentioned above.

The results of those ODS measurements showed that not all of the resonance modes are incited.

Indeed, on every industrial inductors that have been tested here, the resonance modes shown in Fig. 9.b and Fig. 9.c have never been incited, even when the switching frequency and the resonance mode frequencies matched. On the other hand, the resonance mode presented in Fig. 9.a has always been incited when the switching frequency matched the resonance mode frequency. Nevertheless, on every inductors tested here, this resonance mode, even incited, never shown any influence on the acoustic power level.

Finally, the most relevant observation that can be made from those measurements is that the ODS clearly showed that, for every frequency that has been tested, the magnetic core deformed itself according to the breathing mode deflection shape (Fig. 9.d and Fig. 10).

Actually, this phenomenon is not surprising. Indeed, as we mentioned before, in an industrial inductor, magnetostriction forces in the core, electromagnetic forces in the windings and Maxwell forces at the core/air interface are present. Nevertheless, due to the air gaps, the latter are way more important than the others. Moreover, the Maxwell forces are directed along the two columns of the core, and so always excite the breathing mode.

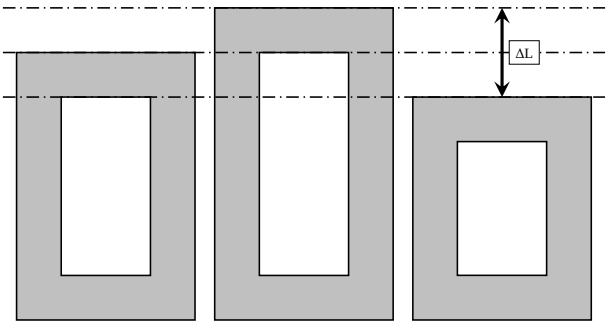

Fig. 10 : industrial inductors deflections
Initial structure (left) – Maximum deflection (center) – minimum deflection (right)

C. From deflections to the emission of sound

As we mentioned it in part B, the magnetic core deforms itself according to a breathing mode deflection shape. Now, the top surface of the industrial inductor core is a plane surface. Moreover, an oscillating plane surface is a noise emission source.

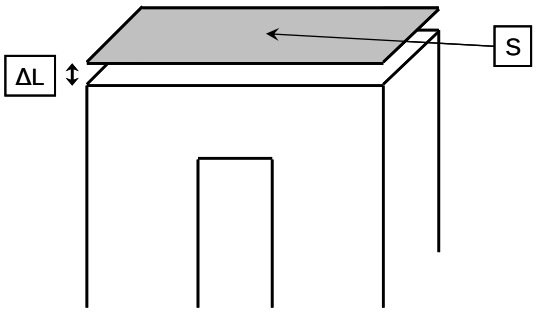

Fig. 11: oscillating surface

According to the notations in Fig. 11, the acoustic power P_{AC} can be expressed as follows:

$$P_{AC} = z_0 \left\langle v^2 \right\rangle S\sigma \tag{11}$$

where z_0 is the acoustic impedance, v is the quadratic velocity, S the area of the oscillating surface and σ is the radiation efficiency. Hence, the sound power level L_w can be calculated by using (12):

$$L_w = 10\log_{10}\left(\frac{P_{AC}}{P_0}\right) \tag{12}$$

where P_0 is the 0 dB reference level and is equal to $10^{-12}W$.

From the ODS measurements, quadratic velocity v can be deduced from the acceleration given by the accelerometers, and the sound power level L_w is simply measured by a microphone placed at 1m in top of the industrial inductor. The results are presented in Table 1.

TABLE 1
COMPARISON BETWEEN MEASURED AND COMPUTED SOUND POWER LEVEL

Frequency	Measurement	Computation
f=1500 Hz	50,8 dB	47,1 dB
f=2700 Hz	52,9 dB	50,7 dB
f=4000 Hz	62,9 dB	66,7 dB

According to the results of that measurement session, the results between measured and calculated sound power level seem in good accordance. Nevertheless, so far, only little DC industrial inductors have been tested, and the same measures have to be done on larger ones.

D. Spring-mass model

According to the observations mentioned in part C, a spring mass model of industrial inductors core could be made by considering the two columns of the core as beams. Hence, those beams can be discretized in N elemental harmonic oscillators, as shown in Fig. 12.

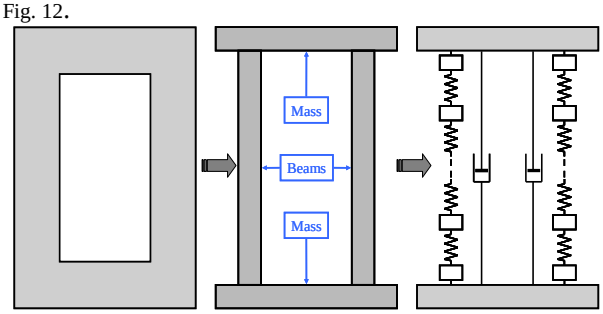

Fig. 12: spring mass model

The values of each elemental mass m_d and spring constant k_d can be expressed as follows:

$$m_d = \frac{m}{N} \tag{13}$$

$$k_d = \frac{E.S}{\left(\frac{L}{N}\right)} \tag{14}$$

where E is the Young modulus, and S and L are the section and the length of a column respectively.

Such an association of elemental harmonic oscillators allows taking into account every natural frequencies of the columns. Moreover, it also allows computing the deflections of the two masses at both sides of the coupled oscillators in the driven case, just by solving classic coupled harmonic oscillators systems.

This model has been validated on classic beams made of pure material (like iron for example) coupled to a mass at the end of the chain. The results have been compared with FE simulations. Nevertheless, the material properties definition that appeared in the FE simulations mentioned in part A appears here.

V. CONCLUSIONS

The design process of magnetic components becomes more and more multi-physical. Hence, it's important for designers to take into account their behaviours in term of electromagnetic, thermal and acoustic. In this paper, three lumped models, an electromagnetic model, a nodal network and a spring-mass model, have been developed for the magnetic, thermal and the vibro-acoustic parts respectively. The aim of our models is to obtain a good compromise between accuracy and time computing. Hence, in the future, these models are coupled to an optimization process in order to obtain an optimal design.

ACKNOWLEDGMENT

This work was supported by MEDEE and Transrail Boige & Vignal (Transformers and inductors supplier). MEDEE is co-financed by European Union. Europe is moving in Nord Pas-de-Calais with the European Regional Development Fund (ERDF)

REFERENCES

[1] W.G. Hurley, W. Wölfle and J.G. Breslin, "Optimized transformer design: Inclusive of high frequency effects", IEEE Transactions on Power Electronics, vol.13, pp. 651-659, July 1998.

[2] P. L. Dowell, "Effects of eddy currents in transformers windings", *Proceeding of IEE*, Vol. 113, no.8, pp1387-1394, Aug. 1966.

[3] X. Nan and C.R. Sullivan, "An improved calculation of proximity effect loss in high frequency windings of round conductors", 34th annual IEEE Power Electronics Specialists Conference, 2003

[4] J. Pyrhönen, T. Jokinen, V. Hrabovcova, "Design of rotating electrical machines", John Wiley & Sons, 2008

[5] G. Swift, T.S. Molinsky and W. Lehn, "A fundamental approach to transformer thermal modelingn part I – theory and equivalent circuit", IEEE Transactions on Power Delivery, Vol. 16, pp.171-175, 2001.

[6] S.A.Ryder, "A simple method for calculating winding temperature gradient in power transformers", IEEE Transactions on Power Delivery, Vol. 16, pp. 171-175, 2001.

[7] M. Rossi, G. Parent, M. Hecquet, V. lanfranchi and M. Bekemans, "Thermal modeling of industrial inductors and transformers associated to the converters", Proceedings of ICEM 2010, Italy, Sept. 2010.

[8] Z. Tang, P. Pillay and A. Omekanda, "Vibration Prediction in Switched Reluctance Motors with Transfer Function Identification From Shaker and Force Hammer Tests", IEEE Transactions on Industry Applications, 39(4):978-985, 2003.

[9] J. Anger, A Daneryd, "Noise in Power Transformers – Models Generation, Transmission and Propagation", UK Magnetics Society, One day seminar, Cardiff, 2009.

[10] P.L. Tilmar, "Noise and Vibration of Electrical Machines", ELSEVIER, 1989

[11] P. Hamberger, "Low Noise Power Transformers – More Energy in large cities with less noise", UK Magnetics Society, One day seminar, Cardiff, 2009

[12] B. Weiser, H. Pfützner, "Relevance of Magnetostriction and Forces for the Generation of Audible Noise of Transformers Cores", IEEE Transactions on Magnetics, 36(5):3759-3777, 2005.